Cellular and Molecular Bioengineering, Vol. 4, No. 2, June 2011 *(© 2011)* pp. 125–137
DOI: 10.1007/s12195-011-0159-x

Single Molecule Detection of One, Two and Multiplex Proteins Involved in DNA/RNA Transaction

YUPENG QIU[1] and SUA MYONG[1,2]

[1]Bioengineering Department, University of Illinois Urbana-Champaign, Champaign, IL, USA; and [2]Institute for Genomic Biology, University of Illinois Urbana-Champaign, Champaign, IL, USA

(Received 15 June 2010; accepted 1 February 2011; published online 11 February 2011)

Associate Editor Yingxiao Wang oversaw the review of this article.

Abstract—Cellular processes involve complex arrangement of proteins engaged in a multitude of reactions, yet in a highly coordinated manner. The level of complexity, however, makes it difficult to investigate the role played by the individual protein constituent. Data taken from the conventional bulk solution methods suffer from ensemble averaging effect in which information from individual molecules is masked. The single molecule detection method overcomes this limitation by offering unique tools for monitoring the activity of individual molecules in isolation and in real-time dynamics. Included in this review are recent articles of single molecule studies representing a diverse array of experimental platforms which demonstrate the power and spectrum of single molecule detection.

Keywords—Single molecule detection, DNA, RNA, Protein, Replication, Transcription, Polymerization, Recombination, FRET, Fluorescence, Magnetic tweezers, Microscope.

INTRODUCTION

Biological processes involve complex architecture of proteins which perform a myriad of reactions in a highly coordinated manner both spatially and temporally. *E. coli* DNA replication alone entails more than 10 proteins including helicase, polymerase, primase and single stranded DNA binding protein (SSB). Each protein has a distinct activity such as unwinding of double stranded DNA, polymerizing complementary strand of DNA and binding and securing single stranded DNA. An accurate assessment of these proteins has tremendous biomedical implications since mutations in human equivalent of such proteins are associated with many types of human cancers. For example, BRCA2 is a DNA binding protein which controls the process of recombination and is found defective in many breast cancer patients and Werner is a helicase which induces premature aging and elevated prevalence of cancer when absent or faltered. The level of complexity however, makes it challenging to investigate the role played by individual component. When taken at an average, even the behavior of one type protein is masked in ensemble readout due to the heterogeneity amongst molecules, dynamic changes both at inter- and intramolecular level and asynchronous reactions. The single molecule detection methods circumvent these limitations by offering unique tools for monitoring the activity of individual molecules in isolation, in real time with a high precision. Included in this review are recent articles of single molecule studies representing a diverse array of experimental platforms including smFRET (single molecule Förster resonance energy transfer), protein induced fluorescence enhancement (PIFE), magnetic tweezers and Slimfield (high-resolution cell imaging microscope). The first four articles are studies focused on single protein component; bacterial RNA polymerase,[54] reverse transcriptase from HIV[23] and RIG-I and RPA from human.[9,37] The "Multi-component Replication Systems" section contains three studies performed on multi-component system found in *E. coli* i.e. single stranded DNA binding protein and RecA[46]; RNA polymerase and helicase/primase,[40] followed by an *in vivo* study where individual participants of *E. coli* replisome are counted with a single protein resolution in *E. coli* cells undergoing cell division.[43] For the purpose of better focus, we chose small set of single molecule studies. For example, we did not include one of the major single molecule techniques, optical trapping which led to exciting recent discoveries on RNA polymerase and nucleosome dynamics.[15,19]

Address correspondence to Sua Myong, Institute for Genomic Biology, University of Illinois Urbana-Champaign, Champaign, IL, USA. Electronic mail: smyong@illinois.edu

1865-5025/11/0600-0125/0 © 2011 Biomedical Engineering Society

SINGLE PROTEIN ACTIVITY REVEALED BY SINGLE MOLECULE DETECTION

Transcription Initiation to Elongation by RNA Polymerase Studied by FRET

Transcription is a process by which a genetic message encoded in DNA is converted to RNA. RNA polymerase (RNAP) is recruited to the promoter site on DNA and initiates the processive elongation, making a full length RNA transcript. A recent study revealed that the rate-limiting step in the transcription process lies in the transition from transcription initiation to elongation of the RNAP.[54] Tang *et al*. used single-Molecule FRET technique to monitor the initiation complex (IC) and elongation complexes (EC) of the model enzyme, T7 RNAP found in bacteriophage. DNA construct was prepared with a pair of FRET fluorophores (Cy3 and Cy5) attached to the T7 promoter region (−4 nt and +17 nt) near the transcription start site (+1 nt) where the T7 RNAP complex is expected to bind. The DNA is immobilized to a polymer coated quartz surface via biotin-neutravidin link (Fig. 1Aa) and the changes in fluorescence intensities resulting from RNAP binding to DNA (Fig. 1Aa) was observed using a wide-field total internal reflection (TIR) microscope setup (Fig. 1Ab).

After forming the DNA–RNAP complex, the transcription reaction was halted at selected positions using incomplete sets of NTPs and derivatives. FRET intensity (E_{corr}) histograms built from hundreds of single molecules revealed distinct FRET peaks indicating discrete conformational states of DNA induced by the corresponding steps of transcription (Fig. 1B). Upon formation of the RNAP–Promoter (R–P) complex, a single low FRET ($E_{corr} \sim 0.12$) peak appeared (Fig. 1B, top left) indicating a large distance between the donor and acceptor (D–A) fluorophores (Fig. 1Aa, left) in R–P.[53] As the RNAP translocates toward the +3 nt direction, the FRET peak migrates to ~0.45 (Fig. 1B, bottom left) and continues to ~0.6 for +9 nt, indicating a shortening of D–A distance within the initiation complex as expected from a sharp bending (~90) in the DNA (Fig. 1Aa, right).[53,58] Beyond +7 nt, the FRET histograms show two distinct peaks: a new lower-FRET population at $E_{corr} \sim 0.3$ along with a higher-FRET population at $E_{corr} \sim 0.6$ (Fig. 1B, top right). The emergence of this new lower FRET state after +7 nt is designated as the EC state and documents the transition from IC to EC, consistent with other T7 RNAP studies.[1,10,12,13,32,58] The lower-FRET peak continues to increase while the higher-FRET peak diminishes as the reaction progresses to just before +12 nt where only the lower-FRET intensity peak remains afterwards (Fig. 1B, bottom right).

Examination of the real-time single-molecule traces displays dynamic changes occurring in sequential steps of transcription; FRET states 1, 2 and 3 as IC 2/3, IC 3/4, and IC 4/5, respectively. The sudden drop followed by a plateau in FRET (0.45) is interpreted as the formation of EC at 12 nt. (Fig. 1C) The mean dwell time, τ of the last state (state 3) set a lower limit on how fast EC formation can occur after 12-nt RNA synthesis, and indicated that the IC-to-EC transition phase is the rate limiting step and that EC formation rate is increased by ~400-fold when the RNA reaches a length of 12 nt.[54]

Being able to resolve the IC-to-EC transition (high to low FRET) state in real time allowed for measurements of the kinetics involved in the EC formation from RNAP complexes halted at +8, +9 and +11 nt position. The kinetic measurements fit to an exponential equation and the reaction rates ($1/\tau$) were measured to show a position-dependent transition from the high-to-low FRET value population (Fig. 1D) which again points to the IC-to-EC transition as the limiting factor in RNA synthesis.

RIG-I Translocation Probed by PIFE (Protein Induced Fluorescence Enhancement)

RIG-I (retinoic acid inducible gene-I) is a major antiviral receptor present in all mammalian cell types.[59] Upon virus entry into cells, RIG-I recognizes viral RNA as a pathogen and triggers antiviral signaling cascade which culminates in type I Interferon production.[59] More specifically, double-stranded RNA (dsRNA) and the 5′-triphosphate moiety uniquely present on viral RNAs are the distinct molecular patterns detected by RIG-I.[16,41] RIG-I is composed of N-terminal tandem CARDs (Caspase Activation Recruitment Domain), central helicase and C-terminal RD (regulatory domain). Although it has been determined that RD detects 5′-triphosphate and CARDs relays the antiviral signal to the downstream partner molecule, the activity of the helicase domain, which is essential for the signaling function has remained elusive.

Recently, we have developed a new single molecule method, termed PIFE (Protein Induced Fluorescence Enhancement) to probe the ATP-driven activity of RIG-I on dsRNA (Fig. 2A). PIFE is distinguished from FRET in that it monitors only the intensity of a single fluorophore where the intensity fluctuations correlate with its proximity to the interacting protein[37] PIFE is presumed to occur when a source of viscosity such as protein comes in the vicinity of a fluorophore, which acts to enhance the quantum yield

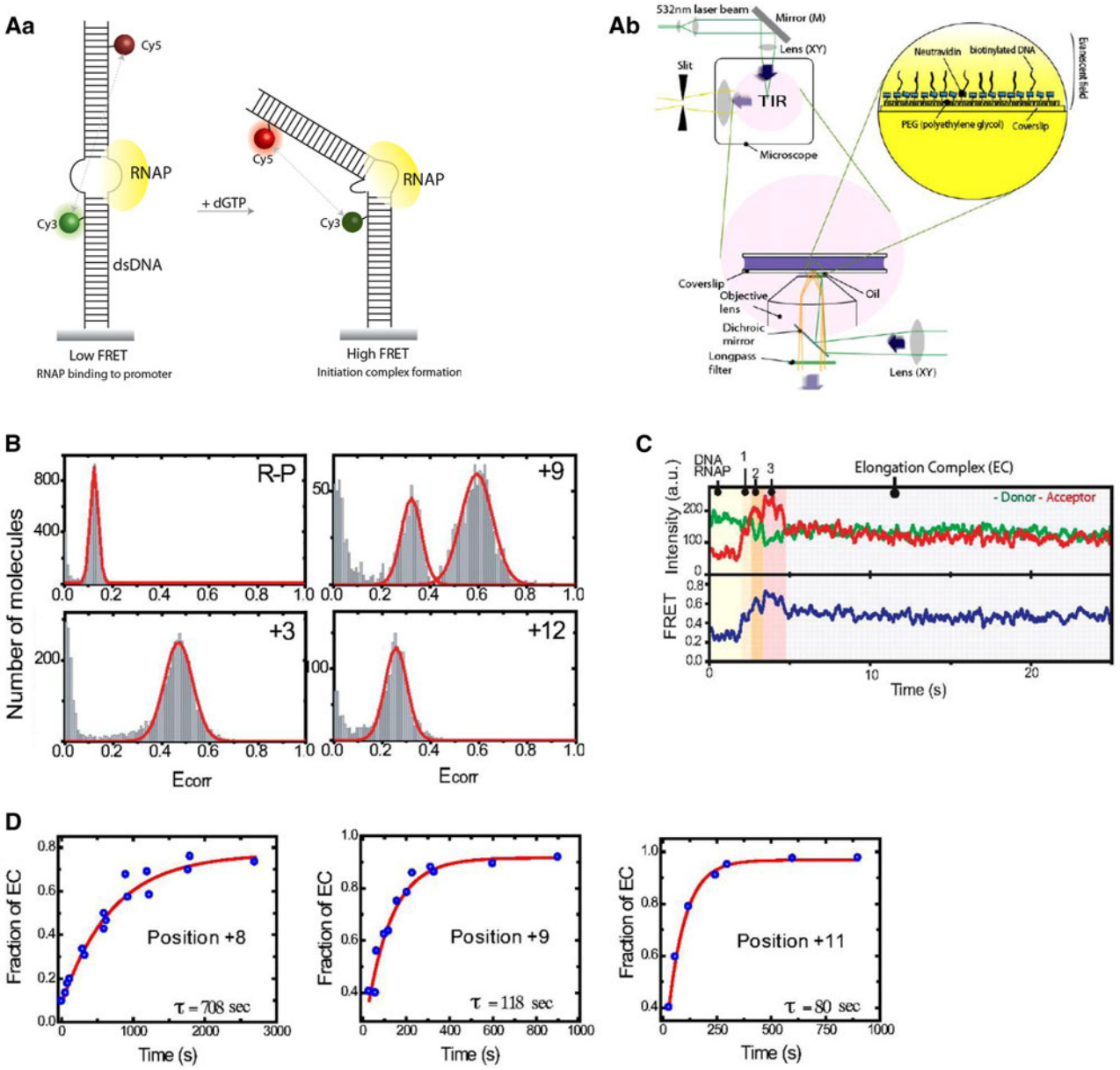

FIGURE 1. T7 RNA polymerase transcription measured by single-molecule FRET. (Aa) DNA construct labeled with Cy3 (green) and Cy5 (red) is prepared for smFRET measurement to monitor conformational changes upon RNAP binding to the promoter sequence during the formation of initialization complex. (Ab) Schematic representation of TIR set up where total internal reflection occurs at the interface between a coverslip and water (side view). (B) FRET histograms show FRET efficiency (corrected for donor leakage) on the *x*-axis and counts of transcribing molecules on the *y*-axis as T7 RNAP transcription was halted at designated positions. (C) Single-molecule trace of anti-correlated donor and acceptor intensities as time trajectory of transcription reaction halted at +12 position. (Upper) Time course of corresponding FRET trace (Lower) The apparent FRET, E_{app}. (D) The fraction of elongation complex (EC) increases with single-exponential kinetics, with the time of reaction providing the indicated mean τ.

of the fluorophore. This photo-enhancement is induced by a protein which reduces the isomerization of fluorophores such as Cy3 to transition from the bright "cis" state to the dark "trans" state.[47] Therefore, PIFE allows study of nucleic acid interacting proteins without having to fluorescently label the protein.[37] In order to study the activity of RIG-I, dsRNA construct end labeled with green (Cy3) fluorophore was tethered to surface in the same way as the previous smFRET study, and RIG-I protein was added with or without ATP (Fig. 2A).

A RIG-I mutant which lacks CARDS domain (RIGh) was first tested since its ATPase activity is efficiently stimulated in the presence of dsRNA.[8] Binding and dissociation of RIGh protein was visualized by a substantial enhancement in signal (PIFE effect)

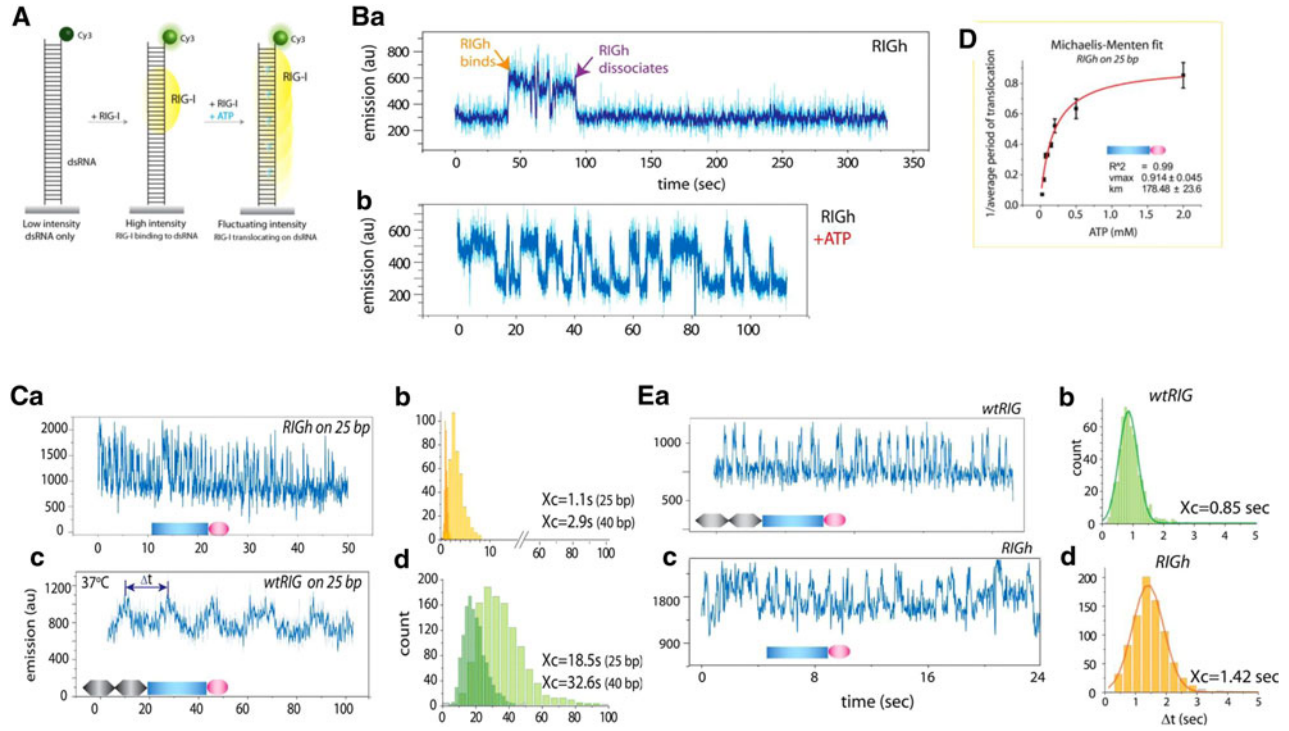

FIGURE 2. PIFE visualization of RIG-I binding and translocation. (A) dsRNA (25 bp) with single fluorophore (DY547) was tethered to surface via biotin-neutravidin. (Ba) Addition of RIGh (CARD-less mutant) resulted in an abrupt increase in emission of the fluorophore, indicating RIGh binding induced by PIFE. (Bb) Addition of RIGh with ATP-induced periodic fluctuation of fluorophore. The signal fluctuation represents RIGh movement along the dsRNA substrate (Ca, c) RIGh and wtRIG translocates on dsRNA at 37 °C. Slower movement by wtRIG indicates an inhibitory role played by CARD (Cb, d) Dwell-time analysis of periods denoted by Δt with a double arrow (Cc) was measured for many molecules and plotted as histograms for RIGh (Cb), wtRIG (Cd) for 25-bp and 40-bp dsRNA. (D) The inverse of average Δt was plotted against an axis of ATP concentration and fitted to the Michaelis–Menten equation. (E) RIG-I translocates on a double strand of 5′-triphosphate RNA at an accelerated speed.

followed by an abrupt decrease in intensity respectively (Fig. 2Ba). With the addition of ATP, the steady signal changed to a periodic fluctuation (Fig. 2Bb), which indicated a repetitive translocational movement of RIGh along the axis of the dsRNA, frequency of which depends on ATP concentration. This fluctuation was also shown to occur much more rapidly at 37 °C (Fig. 2Ca, b). In contrast, the wildtype RIG-I protein wtRIG exhibited a similar fluctuation but at a much subdued frequency as indicated by the dwell time analysis where interval (Δt) between successive peaks were collected from many traces. (Fig. 2Cb, c) The dwell time, Δt, was also shown to be dependent on the length of the RNA oligomer (25 bp and 40 bp) in both cases, supporting that the translocation occurs in the entire length of the dsRNA. The dwell times taken from experiments conducted at varying concentrations of ATP were used to fit Michaelis–Menten equation, which yields V_{max} and K_m values (Fig. 2D). When subject to RNA possessing both of viral signatures, dsRNA and 5′-triphosphate, the wildtype RIG-I exhibits an extremely fast rate of translocation (Fig. 2Ea, b), which is in agreement with the proposed role of CARD in inhibiting ATPase activity of RIG-I.[8] This study demonstrates the first example of an antiviral protein which may use its translocational movement on viral RNA in signaling, perhaps to expose the CARDs for downstream processing and/or to combat other viral proteins along the viral genome.

HIV Reverse Transcription Monitored by Flow Stretching Assay

HIV RT (Human immunodeficiency virus reverse transcriptase) is a multifunctional protein responsible for reverse transcription of its RNA genome into cDNA, and polymerization of DNA using cDNA template. While not a particularly efficient DNA polymerase, HIV-1 RT plays a pivotal role in the HIV-1 life cycle, hence an ideal drug target for clinical treatments. Instead of an accessory helicase that aids in the destabilization of nucleic acid, HIV-1 RT unwinds a large number of stable RNA or DNA secondary structures in the HIV genome during reverse transcription. It is theorized that these structures induce pauses during DNA replication which results in the

recombination of DNA.[38,45] However, the molecular mechanism of how HIV-1 RT replicates through successive secondary structures is not well understood from previous bulk experiments. Single-molecule techniques are advantageous because they offer the ability to monitor multiple turnovers of the polymerase in real time and study the unsynchronized, sequence-dependent dynamics during polymerization reaction.[31,34,50,57]

Kim *et al*. presents the DNA polymerization activity of HIV-RT on DNA template using a single molecule flow-stretching assay whereby the length of the flow-stretched DNA report on the progress and the rate of DNA synthesis (Fig. 3a). Individual single-stranded DNA (ssDNA) templates containing variable DNA sequences and secondary structures are stretched by hydrodynamic flow in a microchannel (Fig. 3a). Each

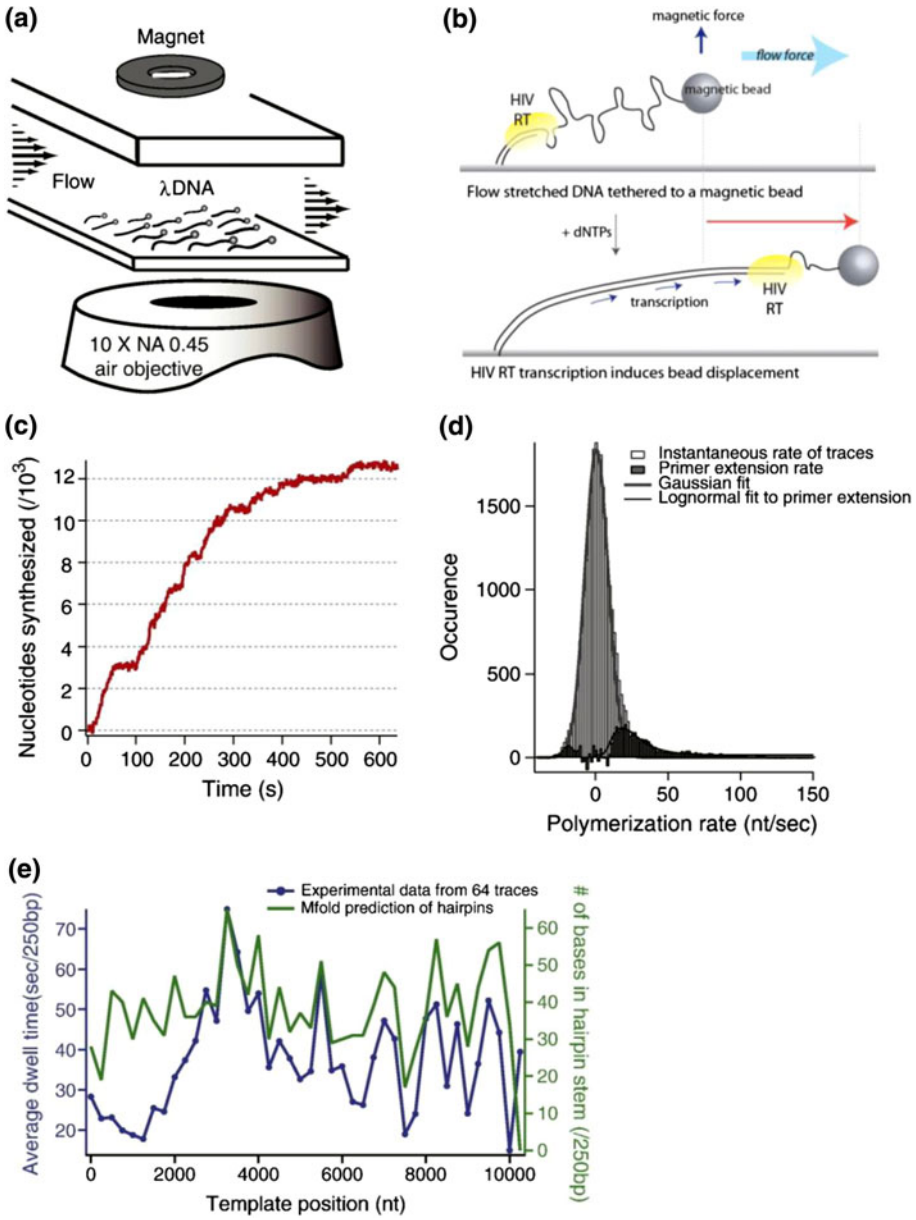

FIGURE 3. DNA replication by HIV-reverse transcriptase on flow-stretched ssDNA (a) Schematic diagram of the experimental setup. (b) Schematic of DNA polymerization by HIV-1 RT resulting in a formation of dsDNA thus lengthening of the DNA visualized by the magnetic bead displacement. (c) Sample trajectory from tracking a DNA-tethered bead over time. (d) Histogram of HIV-1 RT instantaneous polymerization rates from raw polymerization trajectories at a stretching force of 3.0 pN. Effective plateaus are reflected by a Gaussian peak around 0 nt/s. Original distribution subtracted with the Gaussian fit yields a population for the primer extension activity, which is fitted with a log-normal function (black line). (e) Sequence-dependent strand displacement synthesis of HIV-1 RT. Average dwell time (blue dotted line) measured along a λ-DNA template (average of 64 traces) and the number of bases involved in hairpin stems in a 250-base moving window (green continuous line). Correlation analysis between the average dwell time and hairpin stem number density yields a Pearson coefficient of 0.75 up to 10,000 nt.

ssDNA is tagged with biotin on one end to link to the streptavidin-coated surface of the flow cell and with digoxigenin on the other end to tether to a 2.8 μm magnetic bead. Dark-field microscopy is used to monitor the HIV-RT mediated conversion of ssDNA to double-stranded DNA (dsDNA) based on the change in DNA extension (higher for ssDNA) measured by the bead displacement over time as illustrated in Fig. 3b. During the primer extension assay, processive stretches of DNA synthesis were observed along with a slow mode of DNA replication which is shown as a plateau region ranging from a few seconds to 200 s in bead trajectory traces (Fig. 3c). The histogram built from the instantaneous rates of bead trajectories (Fig. 3d) showed a Gaussian shaped peak near 20 nt/s representing the active phase of DNA polymerization and another peak near ~1 nt/s with a long tail resulting from the slow mode synthesis.

The duration of the slow DNA synthesis events are temperature-dependent while the initialization locations are dependent on the locations of hairpin structures on the DNA template. The duration of DNA polymerization events within a 250-base moving window was measured from 64 experimental trajectories (Fig. 3e). The average dwell times (shown as blue dotted line) are measured along the entire DNA template and reflects the relative "strength" of the slow synthesis along the template sequence.[23] A strong correlation was shown between hairpin strength (i.e. length of double strand and G-C content) and the duration of DNA polymerization with a Pearson's correlation coefficient of 0.75 for 10,000 nt. A correction for the thermal melting of nucleotide pairs was also done to allow for the weighting of base pairs, and the resultant Pearson correlation coefficient was improved to 0.87.[23] The high correlation coefficient establishes the hairpin secondary structures as an on/off switch to induce the HIV-1 RT into the slow DNA synthesis mode.

RPA Binding Monitored by Magnetic Tweezers

Single-stranded DNA binding proteins (SSBs) are very important for stabilizing and sequestering ssDNA from nonspecific protein binding. In eukaryotic organisms, the main SSB[18,56] equivalent is Replication Protein A (RPA) and it is integral to many DNA-processing pathways including replication, recombination and repair.[60] RPA subunits bind to ssDNA in a multi-step process with decreasing affinities beginning with an 8–10 nt binding mode and ending in a final 30-nt binding mode. Significant protein conformational changes also accompany the binding process.[4–6,11] Its ssDNA-binding property enables it to capture ssDNA portion of dsDNA, thus destabilize and unwind dsDNA. RPA also directly interacts with variety of other proteins.[11,36]

Using a single-molecule magnetic tweezers (MTs), a recent study by De Vlaminck *et al.* reported on the dynamics of human RPA (hRPA) revealing that hRPA is able to unwind dsDNA with a rate that is exponentially dependent on the torsional stress present in the helical structure of dsDNA.[9] DNA constructs tethered to a paramagnetic bead at one end were anchored to the bottom of a flow cell and video microscopy tracked the bead positions (height) in 3D to measure the change in the end-to-end distance of the DNA (Fig. 4a). The binding affinity of hRPA to ssDNA in various salt concentrations was first tested where the reaction was initiated by flowing in a buffer containing hRPA into the flow cell. The example time trace recorded at a stretching force of 3pN (Fig. 4c) showed an almost immediate increase in the end-to-end distance of the DNA as hRPA proteins bound and stretched the ssDNA. The shape of the association curve allowed analysis that confirmed earlier reports[22] i.e. the hRPA-ssDNA binding has low cooperativity and is independent of NaCl concentrations in the range of 30-600 mM.

The dsDNA-unwinding activity of hRPA is then probed using a dsDNA molecule that has negative supercoils (Fig. 4b). The introduction of a hRPA immediately initiated the unwinding of the helix upon RPA binding and stabilizing the ssDNA bubble. The formation and growth of such bubble lead to a local change in the DNA length as well as changes to the helical twist that can be observed by measuring the change in bead height which can be translated to the number of supercoils in the DNA. A representative binding trace in Fig. 4d showed a nucleation phase (~5 s) and a subsequent increase in the bead height which is interpreted as the progressive duplex unwinding by hRPA proteins that bind and wedge the ssDNA bubble.[27,55] The black line highlights the individual events corresponding to the binding steps of single proteins and formation of the ssDNA bubble. Furthermore, the reaction was abruptly halted at the point where the end-to-end distance of the molecule reached a length of the non-supercoiled molecule, an indication that the reaction has a strong dependence on the presence of torque in DNA (i.e. negative torque from unwinding and positive torque from rewinding).

Finally, the salt dependence of protein dissociation from the ssDNA bubbles in dsDNA was studied by removing the unbound hRPA proteins from the flow cell and the dissociation curves were recorded. Figure 4e shows an example trace of hRPA assembly followed by disassembly at low and high salt concentrations respectively. The disassembly rate of hRPA-dsDNA is faster than from the hRPA-ssDNA

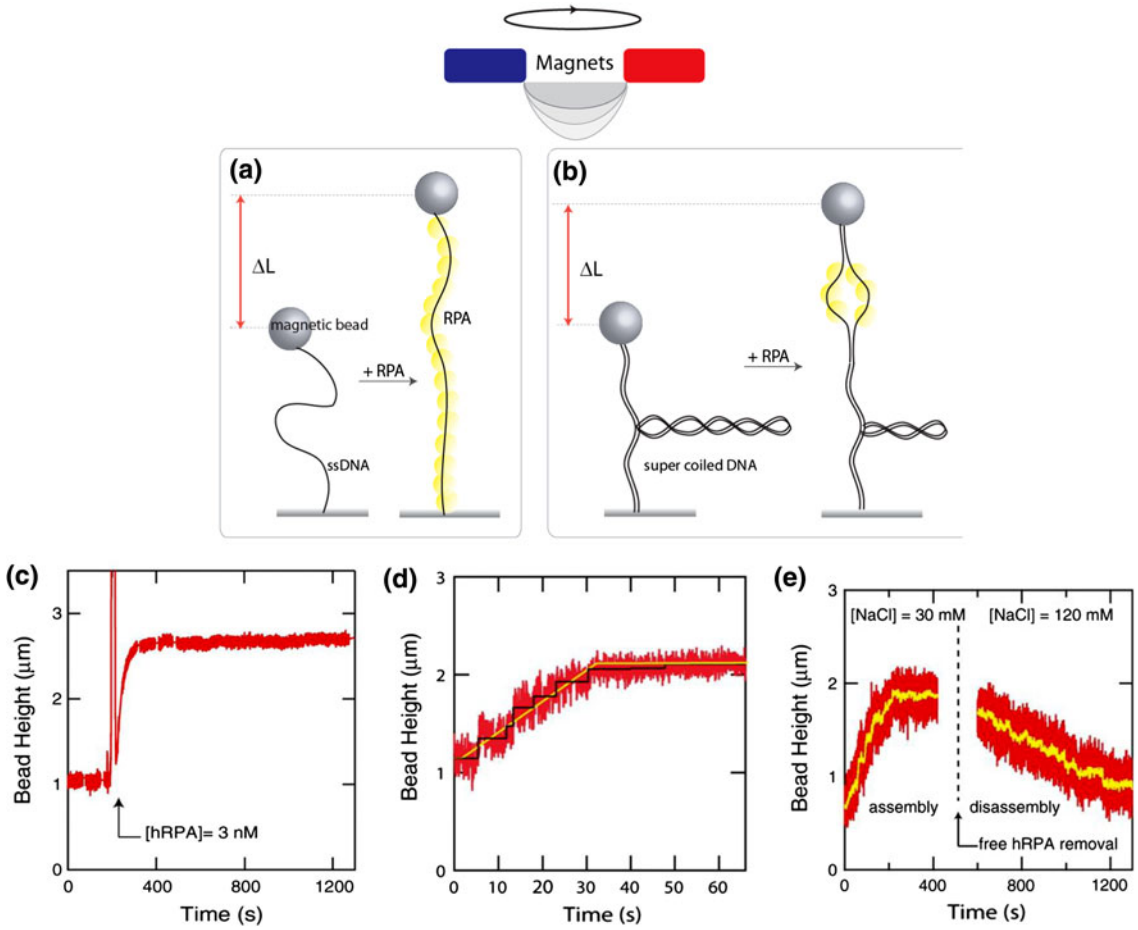

FIGURE 4. hRPA binding to ssDNA probed by magnetic tweezer (a) In a magnetic tweezers setup, a ssDNA and a supercoiled dsDNA molecule (b) is tethered in between a glass slide and a paramagnetic bead. (c) hRPA binding curve taken at a stretching force of 3 pN. The reaction is initiated upon introduction of hRPA in the flow cell. A fast increase in the end-to-end distance is measured. The exponential shape of the binding curve indicates a low binding cooperativity. (d) hRPA binding curve of magnetic bead height plotted against time axis. The binding curve reveals a reaction that progresses linearly in time (yellow line, guide to the eye). Step-like behavior in the binding traces indicates single enzyme binding events (black line, fit based on step finding algorithm). The reaction saturates when the length of the molecule reaches the length of the non-supercoiled DNA. (e) hRPA binding curve at low salt ([NaCl] = 30 mM) followed by dissociation at high salt ([NaCl] = 120 mM).

complex.[9] It's plausible that frequent helix breathing of dsDNA may modulate the dissociation rate and/or that a multi-step dissociation mechanism is involved.

MULTI-COMPONENT REPLICATION SYSTEMS

SSB and RecA Dynamics Visualized by Two and Three Color FRET

The SSB in *E. coli* forms a stable homotetramer which bind to ssDNA with an extremely high affinity.[33] However, it remained unclear as to how the SSB proteins can be efficiently displaced by other proteins to allow subsequent DNA processing. Roy *et al.* employed single-molecule two- and three-color FRET to study the physical interaction between SSB and ssDNA.[46] Two colored smFRET was performed by adding SSB to a partially duplexed DNA possessing Cy3 and Cy5 separated by 69 nt of ssDNA as shown (Fig. 5A). Instead of a constant high FRET expected from wrapping of ssDNA by SSB, they observed rapid FRET fluctuations which represent DNA unwrapping/rewrapping dynamics (Fig. 5A). The source of FRET fluctuation was confirmed as a diffusional migration of SSB rather than the conformational change of SSB by varying the length of ssDNA which yielded FRET values consistent with the dynamic movement of SSB. This marks the first time observation of the dynamic nature of SSB and it offers the mechanistic basis for the function of SSB in recruitment and removal of other ssDNA interacting proteins.

To further characterize the diffusional behavior of SSB on ssDNA, three-color smFRET was used. The SSB was labeled with the donor (Alexa555) and two

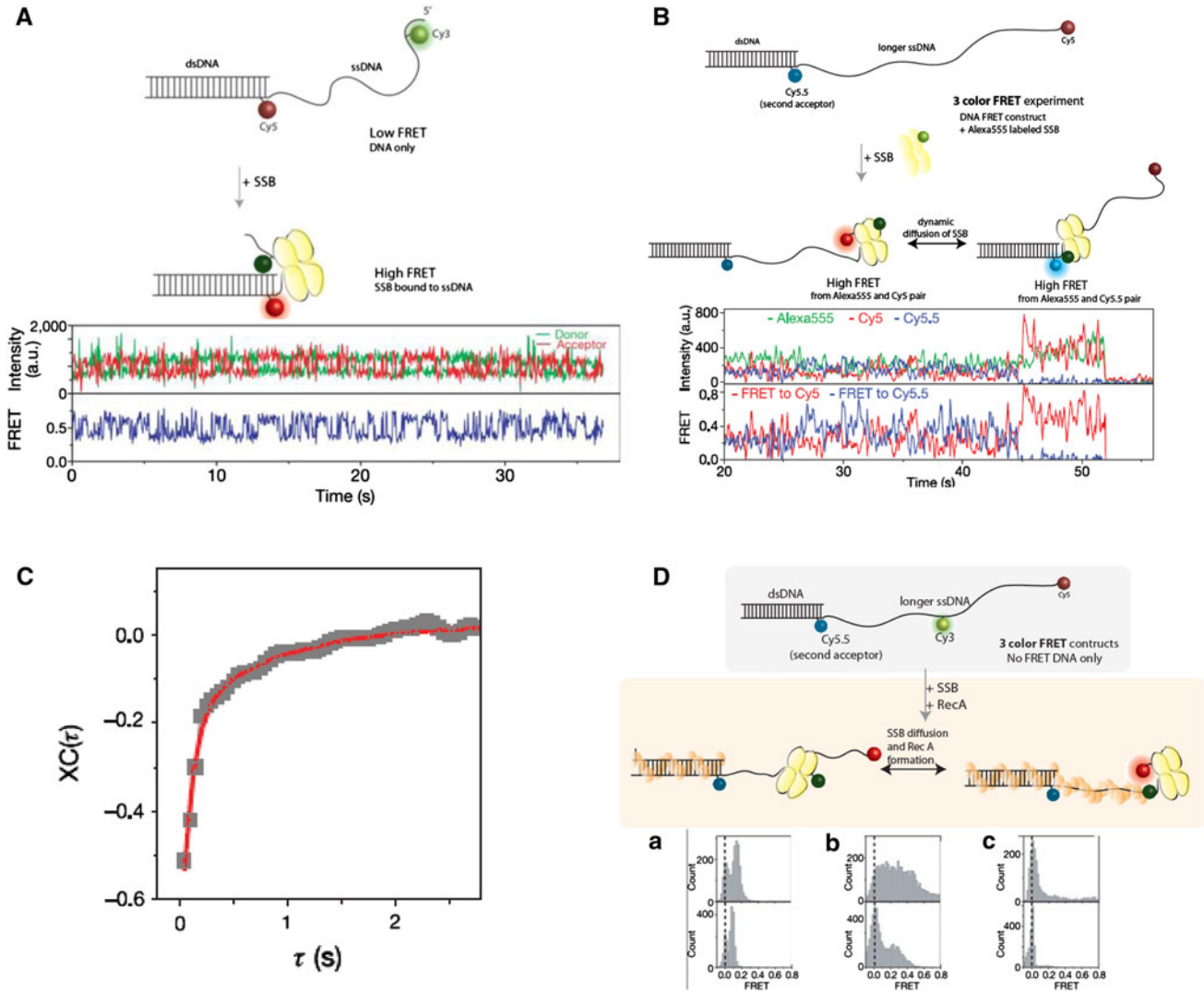

FIGURE 5. Diffusional migration of SSB on ssDNA visualized by three color smFRET. (A) Partially duplexed DNA with a long ssDNA tail on the 5′ end separates the donor and acceptor fluorophores. Addition of SSB results in rapid fluctuations in FRET indicating diffusional motion of SSB on the ssDNA. (B) Three color FRET experiment was designed with Cy3 labeled SSB on dual acceptor labeled DNA. Time traces of three color intensities and the FRET efficiencies ($E_{app,5}$, $E_{app,5.5}$) display diffusion of donor-labelled SSB to acceptor-labelled ends of a ssDNA. (C) The average cross-correlation XC(τ) between $E_{app,5}$ and $E_{app,5.5}$ time traces fit with a bi-exponential decay (red), demonstrating anti-correlated fluctuations. (D) Top panel, schematic of reaction steps; middle panel, $E_{app,5}$ histograms; bottom panel, $E_{app,5.5}$ histograms. (Da) DNA construct with Cy3, Cy5 and Cy5.5. prepared for three color FRET experiment. (Db) Removal of RecA filament from ssDNA and addition of SSB to ssDNA tail. (Dc) RecA filament re-growth on ssDNA tail.

different acceptors, Cy5 and Cy5.5 were attached to the two ends of a $(dT)_{130}$ (Fig. 5B). Rapid fluctuations of FRET efficiencies to either acceptor were observed in a mutually exclusive manner, confirming that SSB indeed migrate from one end to the other end of ssDNA axis. The average cross-correlation between the two acceptor time traces were fit to a bi-exponential decay demonstrating that the fluctuations were anti-correlated (Fig. 5C).[46]

In order to probe how SSB modulates the formation of RecA protein in the recombinational repair pathway,[24–26,44,48] three-color FRET assay was designed to monitor the effect of SSB diffusion in the formation of the RecA filament on ssDNA. A partial duplex DNA was used with a 96 nucleotide 3′ tail, $(dT)_{95}$, labeled at positions 0, 30 and 95 with Cy5.5, Cy3 and Cy5, respectively (Fig. 5D, top panel, bottom panel a). The apparent FRET efficiencies drop to zero as RecA-ATPγS (non-hydrolyzable ATP analog) filament formed. The unbound RecA and the filament formed around the ssDNA tail is flushed out, leaving the RecA filament bound to dsDNA. Upon addition of SSB, DNA displays higher FRET with a broad distribution that reflects SSB binding and diffusion at various

locations along the ssDNA (Fig. 5D, middle panel left, bottom panel b). The RecA-ATPγS filament remaining on the dsDNA then serves as the nucleation cluster for filament elongation on the 3′ ssDNA tail[21] for the newly formed RecA filament (Fig. 5D, middle panel right, bottom panel c). As the filament elongates, the SSB is rapidly replaced until the ssDNA tail is completely coated with the RecA filament again and the apparent FRET efficiencies returned to zero. The prebound SSB promoted RecA formation by 40-fold in regions of DNA with secondary structures. The clever use of three-colored FRET allowed for imaging of two independent activities mediated by RecA and SSB and thereby showing how SSB can promote subsequent steps of DNA processing by RecA.

T7 Replication System Studied by FRET

During DNA replication of T7 bacteriophage, two DNA polymerases work as a partner; one works on the continual replication of the leading strand while the other synthesizes discontinuous Okazaki fragments at the lagging strand.[2,39] A recent study by Pandey *et al.* used single molecule assay in combination with kinetic biochemical analysis to investigate how the two strands can be replicated at the same net rate when the lagging strand requires an additional time for priming events and recycling of its polymerase.[40] In contrast to the previous finding which reported T7 replisome pausing to allow extra time for primer synthesis,[14,31] the current article indicates no evidence of pausing and demonstrates that the difference instead is compensated by a slower rate of leading strand synthesis limited by the speed of the helicase. They also report a direct visualization of a loop formation at the lagging strand mediated by a continuous contact between the primase and the priming sequence.

The study of DNA unwinding kinetics is performed using synthetic replication-fork substrates with and without the T7 priming sequence labeled with donor (Cy3) and acceptor (Cy5) as shown (Fig. 6A). Single Molecule FRET assays were performed to monitor the process of DNA unwinding and synthesis (Fig. 6A). The increase in the donor (Cy3, green) and the concomitant decrease in the acceptor (Cy5, red) signal resulted from the unwinding by the helicase coupled with the synthesis by the polymerase in both DNA constructs. The lack of any pausing events in the single molecule trace analysis suggests that the T7 replisome does not pause during primer synthesis.[40] Furthermore, a high-resolution sequencing gel which captures any accumulation of intermediate DNA product as a result of possible replisome pausing shows that no such product exists for the priming or the control forks.[40] The overall conclusion indicates that DNA synthesis occurs concurrently with the primer synthesis, thus indicating a possible formation of a priming loop on the lagging-strand.

The formation of a primer loop during lagging-strand synthesis was examined with single-molecule FRET experiments. Donor (Cy3) and acceptor (Cy5) fluorophores were located 40 base pairs apart on the lagging-strand template(Fig. 6B). Prior to unwinding, the D–A distance is long and no FRET was observed (Fig. 6C, top panel a). As the T7 replisome loads on DNA and start unwinding, the Cy3 signal shows an increased intensity (Fig. 6C, top panel b) due to PIFE[37] resulting from the proximity of the protein complex to the fluorophore.[47] As the replisome unwinds the DNA, high FRET emerges providing evidence for the formation of a priming loop enabled by the primase which maintains contact with the priming sequence during replication (Fig. 6C, top panel c). The priming loop grows in size as the unwinding process continues and the donor and acceptor move away from each other and the FRET value decreases (Fig. 6C, top panel d, middle panels). Finally, the FRET signal disappears upon the completion of the unwinding reaction and the fluorescently labeled DNA strand is released from the surface.

Additional transient-state kinetic assays using sequencing gels measured the DNA synthesis rate of the leading strand synthesis by the T7 replisome and found that it was slower than the DNA synthesis rate of the lagging-strand by the T7 DNA polymerase, which is consistent with the notion that the DNA synthesis rate is limited by the speed of the helicase.[52] The ability of the T7 replisome to make primers ahead of time during DNA synthesis coupled with the faster rate of lagging strand synthesis allows the T7 replisome to proceed without pausing.

E. coli Replisome Complex Imaged in Living Cells by Slimfield Microscope

The process of replication involves a multiprotein replisome complex which has been well characterized *in vitro* as demonstrated by the articles aforementioned but the compositional and stoichiometric organization of the replisome proteins in living cells remain poorly understood. Using an improved fluorescence microscopy protocol developed for the single-molecule sensitivity and millisecond temporal resolution, a recent study aimed to investigate the active replisome architecture in living cells.[43] The new protocol, termed "Slimfield" uses a compact Gaussian laser excitation field that encompasses single cells, greatly enhancing the excitation intensity without disrupting the cells' ability to replicate.[42] Using fully functional fluorescent YPet derivatives of *E. coli* replisome components, the

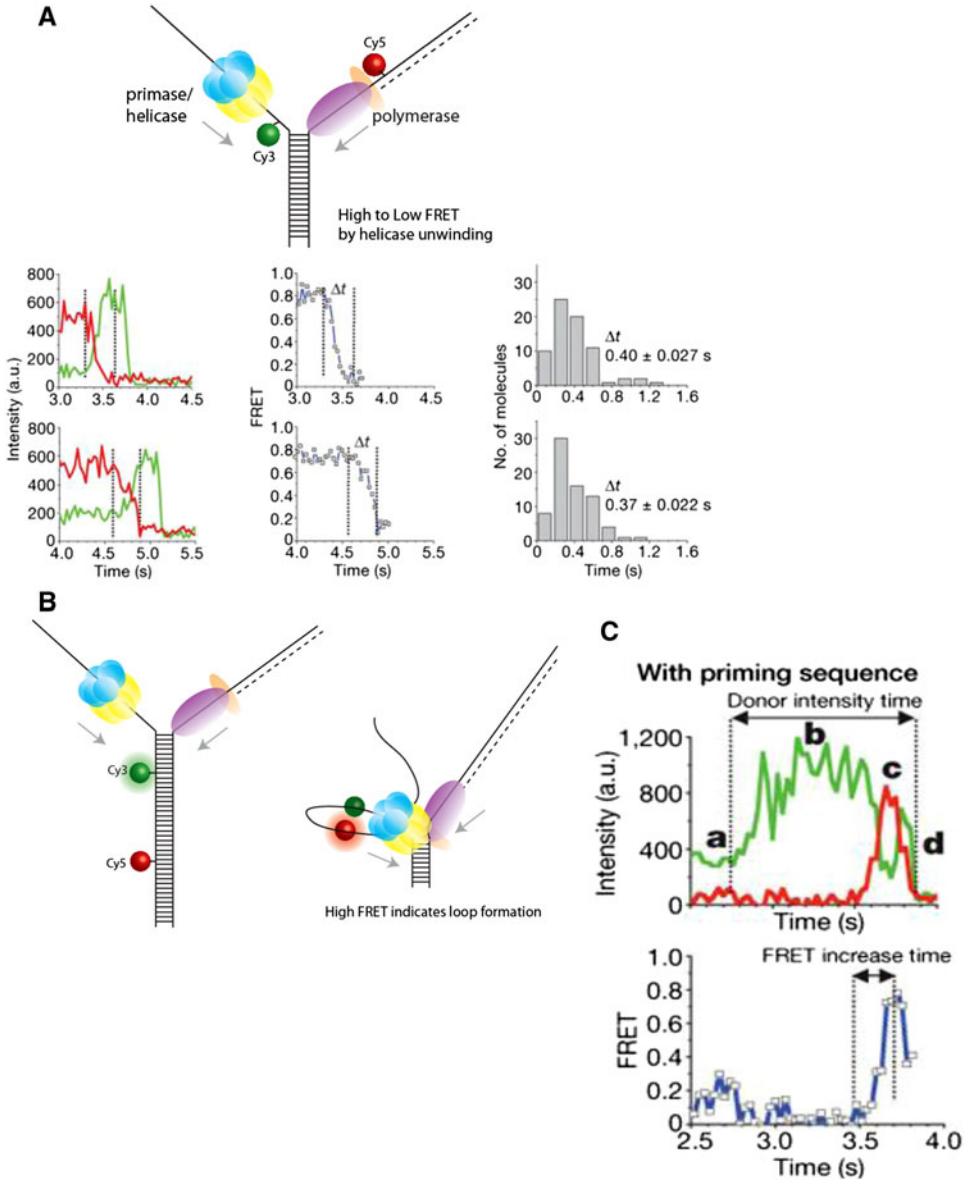

FIGURE 6. DNA unwinding and synthesis. (A) Bottom left graph: representative Cy3 and Cy5 intensity traces showing DNA unwinding on priming (top) and control without the priming sequence (bottom) substrates by single-molecule FRET with T7 replisome. Bottom middle graphs: FRET time courses; Bottom right graphs: dwell-time histograms. Priming and control substrates show similar FRET decrease times (Δt) due to unwinding and synthesis. (B) Fluorescently labelled DNA fork to investigate the priming loop. (C) Top: Cy3 (donor, green) and Cy5 (acceptor, red) intensity time traces during DNA synthesis by T7 replisome. Bottom: plot of FRET efficiency against time.

Slimfield imaging provided quantitative detection of single fluorescent molecules at 3 ms time resolution (Fig. 7A).

The stoichiometry of the replisome is estimated from the image frames (averaged over 90 ms) by finding "hotspots" for localization of a given YPet fusion protein. Stepwise intensity changes representing photobleaching steps were detected from each spot in every individual image frame to deduce the number of molecules in each spot (Fig. 7B). The step spacing measurements were done using an edge-preserving filter[7,51] and analyzed with Fourier spectral analysis. The similarities between the *in vivo* intensity step traces and *in vitro* measurement using purified YPet[28–30] suggested that single-molecule stoichiometry determination can be achieved via analysis of intensity measurements collected prior to photobleaching.[43]

In most of the cells, the sister replisomes are separable and associated with independent forks, resulting in a bimodal 1:2 distribution. When the replisomes are separated by a distance that is smaller than the diffraction limit of light, the fluorescent

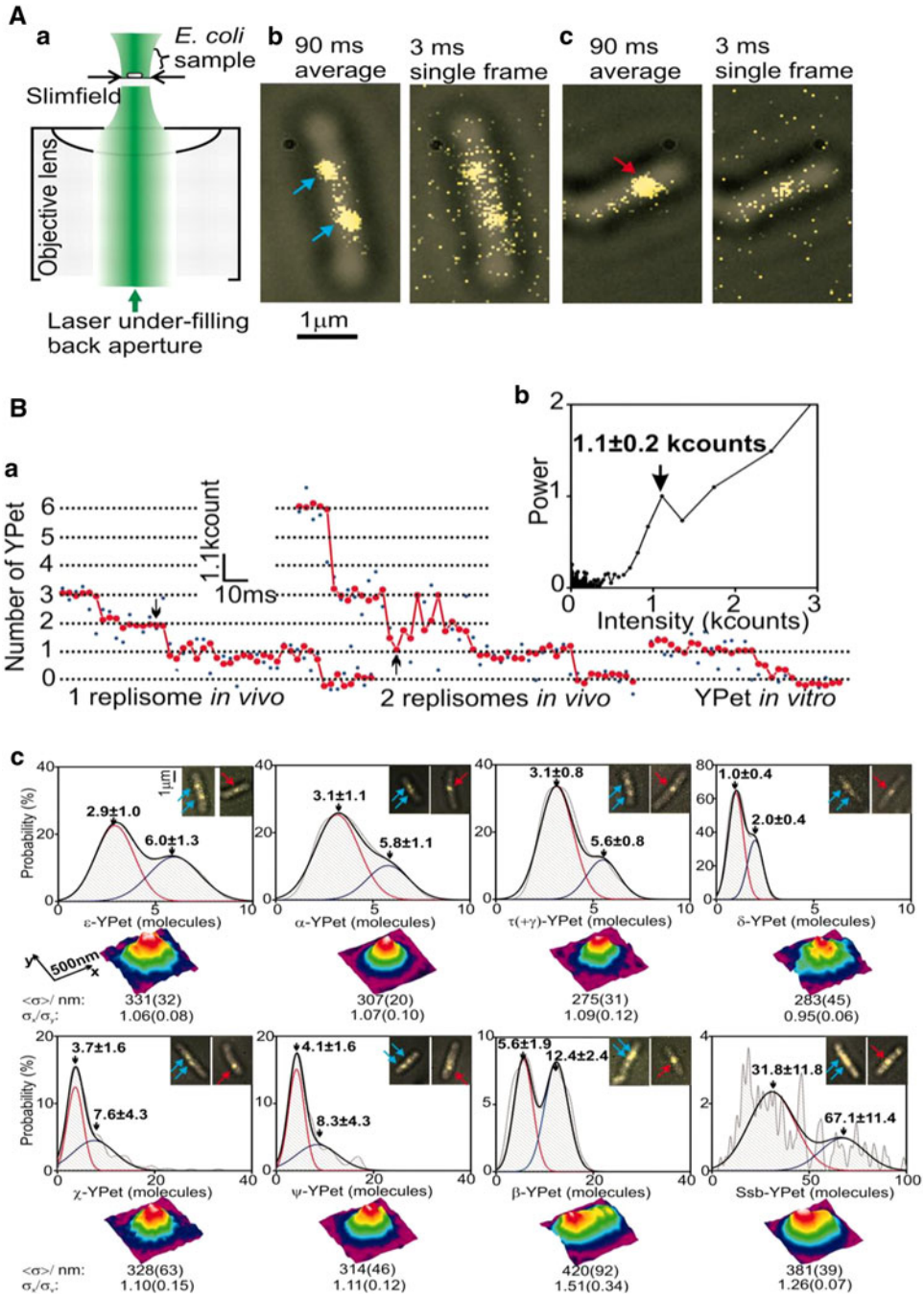

FIGURE 7. Slimfield microscopy and photobleaching analysis. (Aa) Slimfield schematic. A laser underfills the back aperture of an objective lens, generating an intense Gaussian field at the sample large enough to image single *E. coli*. (Ab and Ac) Overlaid bright-field (gray) and 90-ms frame-averaged fluorescence images (yellow) of ε-YPet strain; arrows indicate spots with a stoichiometry of ~3 [cyan, (B)] and ~6 [red, (C)] ε-YPet molecules, with corresponding single 3-ms frames taken after 45 ms, showing that stochastic photobleaching generates different brightnesses. (Ba) Raw intensity (blue) and filtered data (red) for a putative single (left panel) and double (right panel) replisome spot with surface-immobilized YPet *in vitro*; arrows indicate the 45-ms point. (Bb) Fourier spectral analysis for a photobleach trace of the ε-YPet strain with mean ± SD peak indicated for brightness of a single YPet. (C) Stoichiometries of replisome components and spatial distributions.

molecules are observed as a single spot. Examination of various YPet strains from different components of the replisome and analysis of their stoichiometry distributions revealed interesting information on their involvement in replication. Three copies of the clamp loader component, τ, which also oligomerizes Pol III,[20] was associated with the replisome while the alternative clamp loader constituent, γ, was nonessential.[3] The SSB

tetramers which bind to unwound DNA on the lagging-strand showed a broad distribution of stoichiometries (Fig. 7C) where the number of SSB molecules is proportional to the length of ssDNA at the replication fork.[35]

Analysis on the stoichiometry of the dimeric β sliding clamp suggests that three β dimers are continuously associated with the active Pol III or the clamp loader. This observation provides strong evidence that the core replisome contains three, not two, Pol IIIs are associated with a clamp loader whose three copies of τ also trimerize Pol III. The authors suggest that the third polymerase is waiting to be loaded onto the next lagging strand primer.[43]

CONCLUSION

Recent advances in single molecule detection techniques have contributed to unraveling the dynamic features of biological processes in molecular details as represented in this review. The ability to monitor the intrinsic activity of a protein at a single molecule resolution allows one to dissect complex biological machinery into individual constituents and investigate one component at a time. As demonstrated by Roy *et al.*[46] where the role of SSB diffusion was studied in the context of RecA filament formation using three color FRET, one can extend the single molecule approaches to multi-color and multi-protein dimensions. Furthermore, super resolution imaging techniques such as PALM,[49] STORM[17] and the Slimfield[43] provides single molecule images inside of cells in real time. When performed in parallel, the combined information from both types of imaging will yield complementary information which bridges the gap between *in vitro* and *in vivo* measurement.

REFERENCES

[1]Bandwar, R. P., G. Q. Tang, and S. S. Patel. Sequential release of promoter contacts during transcription initiation to elongation transition. *J. Mol. Biol.* 360(2):466–483, 2006.

[2]Benkovic, S. J., A. M. Valentine, and F. Salinas. Replisome-mediated DNA replication. *Annu. Rev. Biochem.* 70:181–208, 2001.

[3]Blinkova, A., *et al.* The *Escherichia coli* DNA polymerase III holoenzyme contains both products of the dnaX gene, tau and gamma, but only tau is essential. *J. Bacteriol.* 175(18):6018–6027, 1993.

[4]Bochkareva, E., *et al.* Structure of the major single-stranded DNA-binding domain of replication protein A suggests a dynamic mechanism for DNA binding. *EMBO J.* 20(3):612–618, 2001.

[5]Bochkareva, E., *et al.* Structure of the RPA trimerization core and its role in the multistep DNA-binding mechanism of RPA. *EMBO J.* 21(7):1855–1863, 2002.

[6]Cai, L., *et al.* Structural characterization of human RPA sequential binding to single-stranded DNA using ssDNA as a molecular ruler. *Biochemistry* 46(28):8226–8233, 2007.

[7]Chung, S. H., and R. A. Kennedy. Forward-backward non-linear filtering technique for extracting small biological signals from noise. *J. Neurosci. Methods* 40(1):71–86, 1991.

[8]Cui, S., *et al.* The C-terminal regulatory domain is the RNA 5′-triphosphate sensor of RIG-I. *Mol. Cell.* 29(2):169–179, 2008.

[9]De Vlaminck, I., *et al.* Torsional regulation of hRPA-induced unwinding of double-stranded DNA. *Nucleic Acids Res.* 2010.

[10]Durniak, K. J., S. Bailey, and T. A. Steitz. The structure of a transcribing T7 RNA polymerase in transition from initiation to elongation. *Science* 322(5901):553–557, 2008.

[11]Fanning, E., V. Klimovich, and A. R. Nager. A dynamic model for replication protein A (RPA) function in DNA processing pathways. *Nucleic Acids Res.* 34(15):4126–4137, 2006.

[12]Gong, P., E. A. Esposito, and C. T. Martin. Initial bubble collapse plays a key role in the transition to elongation in T7 RNA polymeras. *J. Biol. Chem.* 279(43):44277–44285, 2004.

[13]Guo, Q., *et al.* Major conformational changes during T7RNAP transcription initiation coincide with, and are required for, promoter release. *J. Mol. Biol.* 353(2):256–270, 2005.

[14]Hamdan, S. M., *et al.* Dynamics of DNA replication loops reveal temporal control of lagging-strand synthesis. *Nature* 457(7227):336–339, 2009.

[15]Hodges, C., *et al.* Nucleosomal fluctuations govern the transcription dynamics of RNA polymerase II. *Science* 325(5940):626–628, 2009.

[16]Hornung, V., *et al.* 5′-Triphosphate RNA is the ligand for RIG-I. *Science* 314(5801):994–997, 2006.

[17]Huang, B., *et al.* Whole-cell 3D STORM reveals interactions between cellular structures with nanometer-scale resolution. *Nat. Methods* 5(12):1047–1052, 2008.

[18]Iftode, C., Y. Daniely, and J. A. Borowiec. Replication protein A (RPA): the eukaryotic SSB. *Crit. Rev. Biochem. Mol. Biol.* 34(3):141–180, 1999.

[19]Jin, J., *et al.* Synergistic action of RNA polymerases in overcoming the nucleosomal barrier. *Nat. Struct. Mol. Biol.* 17(6):745–752, 2010.

[20]Johnson, A., and M. O'Donnell. Cellular DNA replicases: components and dynamics at the replication fork. *Annu. Rev. Biochem.* 74:283–315, 2005.

[21]Joo, C., *et al.* Real-time observation of RecA filament dynamics with single monomer resolution. *Cell* 126(3):515–527, 2006.

[22]Kim, C., and M. S. Wold. Recombinant human replication protein A binds to polynucleotides with low cooperativity. *Biochemistry* 34(6):2058–2064, 1995.

[23]Kim, S., C. M. Schroeder, and X. S. Xie. Single-molecule study of DNA polymerization activity of HIV-1 reverse transcriptase on DNA templates. *J. Mol. Biol.* 395(5):995–1006, 2010.

[24]Kowalczykowski, S. C. Initiation of genetic recombination and recombination-dependent replication. *Trends Biochem. Sci.* 25(4):156–165, 2000.

[25]Kowalczykowski, S. C., *et al*. Biochemistry of homologous recombination in *Escherichia coli*. *Microbiol. Rev*. 58(3): 401–465, 1994.
[26]Kuzminov, A. Recombinational repair of DNA damage in *Escherichia coli* and bacteriophage lambda. *Microbiol. Mol. Biol. Rev*. 63(4):751–813, 1999; (table of contents).
[27]Lao, Y., C. G. Lee, and M. S. Wold. Replication protein A interactions with DNA. 2. Characterization of double-stranded DNA-binding/helix-destabilization activities and the role of the zinc-finger domain in DNA interactions. *Biochemistry* 38(13):3974–3984, 1999.
[28]Leake, M. C., *et al*. The elasticity of single kettin molecules using a two-bead laser-tweezers assay. *FEBS Lett*. 535(1–3):55–60, 2003.
[29]Leake, M. C., *et al*. The elasticity of single titin molecules using a two-bead optical tweezers assay. *Biophys. J*. 87(2): 1112–1135, 2004.
[30]Leake, M. C., *et al*. Stoichiometry and turnover in single, functioning membrane protein complexes. *Nature* 443(7109): 355–358, 2006.
[31]Lee, J. B. DNA primase acts as a molecular brake in DNA replication. *Nature* 439(7076):621–624, 2006.
[32]Liu, C., and C. T. Martin. Promoter clearance by T7 RNA polymerase. Initial bubble collapse and transcript dissociation monitored by base analog fluorescence. *J. Biol. Chem*. 277(4):2725–2731, 2002.
[33]Lohman, T. M., and M. E. Ferrari. *Escherichia coli* single-stranded DNA-binding protein: multiple DNA-binding modes and cooperativities. *Annu. Rev. Biochem*. 63:527–570, 1994.
[34]Maier, B., D. Bensimon, and V. Croquette. Replication by a single DNA polymerase of a stretched single-stranded DNA. *Proc. Nat. Acad. Sci. U.S.A*. 97(22):12002–12007, 2000.
[35]McInerney, P., and M. O'Donnell. Replisome fate upon encountering a leading strand block and clearance from DNA by recombination proteins. *J. Biol. Chem*. 282(35): 25903–25916, 2007.
[36]Mer, G., *et al*. Structural basis for the recognition of DNA repair proteins UNG2, XPA, and RAD52 by replication factor RPA. *Cell* 103(3):449–456, 2000.
[37]Myong, S., *et al*. Cytosolic viral sensor RIG-I is a 5′-triphosphate-dependent translocase on double-stranded RNA. *Science* 323(5917):1070–1074, 2009.
[38]Negroni, M., and H. Buc. Mechanisms of retroviral recombination. *Annu. Rev. Genet*. 35:275–302, 2001.
[39]O'Donnell, M. Replisome architecture and dynamics in *Escherichia coli*. *J. Biol. Chem*. 281(16):10653–10656, 2006.
[40]Pandey, M., *et al*. Coordinating DNA replication by means of priming loop and differential synthesis rate. *Nature* 462(7275):940–943, 2009.
[41]Pichlmair, A., *et al*. RIG-I-mediated antiviral responses to single-stranded RNA bearing 5′-phosphates. *Science* 314(5801):997–1001, 2006.
[42]Plank, M., G. H. Wadhams, and M. C. Leake. Millisecond timescale slimfield imaging and automated quantification of single fluorescent protein molecules for use in probing complex biological processes. *Integr. Biol. (Camb)* 1(10):602–612, 2009.
[43]Reyes-Lamothe, R., D. J. Sherratt, and M. C. Leake. Stoichiometry and architecture of active DNA replication machinery in *Escherichia coli*. *Science* 328(5977):498–501, 2010.
[44]Roca, A. I., and M. M. Cox. RecA protein: structure, function, and role in recombinational DNA repair. *Prog. Nucleic Acid Res. Mol. Biol*. 56:129–223, 1997.
[45]Roda, R. H., *et al*. Role of the reverse transcriptase, nucleocapsid protein, and template structure in the two-step transfer mechanism in retroviral recombination. *J. Biol. Chem*. 278(34):31536–31546, 2003.
[46]Roy, R., *et al*. SSB protein diffusion on single-stranded DNA stimulates RecA filament formation. *Nature* 461(7267):1092–1097, 2009.
[47]Sanborn, M. E., *et al*. Fluorescence properties and photophysics of the sulfoindocyanine Cy3 linked covalently to DNA. *J. Phys. Chem. B* 111(37):11064–11074, 2007.
[48]Shereda, R. D., *et al*. SSB as an organizer/mobilizer of genome maintenance complexes. *Crit. Rev. Biochem. Mol. Biol*. 43(5):289–318, 2008.
[49]Shroff, H., H. White, and E. Betzig. *Photoactivated localization microscopy (PALM) of adhesion complexes*. *Curr. Protoc. Cell Biol*., 2008. Chapter 4: p. Unit 4 21.
[50]Shundrovsky, A. A single-molecule technique to study sequence-dependent transcription pausing. *Biophys. J*. 87(6): 3945–3953, 2004.
[51]Smith, D. A. A quantitative method for the detection of edges in noisy time-series. *Philos. Trans. R. Soc. B-Biol. Sci*. 353(1378):1969–1981, 1998.
[52]Stano, N. M., *et al*. DNA synthesis provides the driving force to accelerate DNA unwinding by a helicase. *Nature* 435(7040):370–373, 2005.
[53]Tang, G. Q., and S. S. Patel. T7 RNA polymerase-induced bending of promoter DNA is coupled to DNA opening. *Biochemistry* 45(15):4936–4946, 2006.
[54]Tang, G. Q., *et al*. Real-time observation of the transition from transcription initiation to elongation of the RNA polymerase. *Proc. Nat. Acad. Sci. U.S.A*. 106(52):22175–22180, 2009.
[55]Treuner, K., U. Ramsperger, and R. Knippers. Replication protein A induces the unwinding of long double-stranded DNA regions. *J. Mol. Biol*. 259(1):104–112, 1996.
[56]Wold, M. S. Replication protein A: a heterotrimeric, single-stranded DNA-binding protein required for eukaryotic DNA metabolism. *Annu. Rev. Biochem*. 66:61–92, 1997.
[57]Wuite, G. J., *et al*. Single-molecule studies of the effect of template tension on T7 DNA polymerase activity. *Nature* 404(6773):103–106, 2000.
[58]Yin, Y. W., and T. A. Steitz. Structural basis for the transitionfrom initiation to elongation transcription in T7 RNA polymerase. *Science* 298(5597):1387–1395, 2002.
[59]Yoneyama, M., *et al*. The RNA helicase RIG-I has an essential function in double-stranded RNA-induced innate antiviral responses. *Nat. Immunol*. 5(7):730–737, 2004.
[60]Zou, Y., *et al*. Functions of human replication protein A (RPA): from DNA replication to DNA damage and stress responses. *J. Cell. Physiol*. 208(2):267–273, 2006.